Journal of Biomedical Optics

SPIEDigitalLibrary.org/jbo

In situ histology of mice skin through transfer learning of tissue energy interaction in optical coherence tomography

Debdoot Sheet
Amrita Chaudhary
Sri Phani Krishna Karri
Debnath Das
Amin Katouzian
Provas Banerjee
Nassir Navab
Jyotirmoy Chatterjee
Ajoy K. Ray

SPIE

In situ histology of mice skin through transfer learning of tissue energy interaction in optical coherence tomography

Debdoot Sheet,[a] Amrita Chaudhary,[a] Sri Phani Krishna Karri,[a] Debnath Das,[a] Amin Katouzian,[c] Provas Banerjee,[d] Nassir Navab,[c] Jyotirmoy Chatterjee,[a] and Ajoy K. Ray[b]
[a]Indian Institute of Technology Kharagpur, School of Medical Science and Technology, Kharagpur 721302, India
[b]Indian Institute of Technology Kharagpur, Department of Electronics and Electrical Communication Engineering, Kharagpur 721302, India
[c]Technische Universität München, Computer Aided Medical Procedures, 85748 München, Germany
[d]Banerjee's Biomedical Research Foundation, Kolkata 700005, India

Abstract. Tissue characterization method in optical coherence tomography (OCT) for *in situ* histology of soft tissues is presented and demonstrated for mice skin. OCT allows direct noninvasive visualization of subsurface anatomy. It is currently used for *in situ* investigation of lesions in skin, vessels, retinal layers, oral, and bronchial cavitities. Although OCT images present high resolution information about tissue morphology, reporting requires a reader experienced in interpretation of the images, viz., identification of anatomical layers and structures constituting the organ based on OCT speckle appearance. Our approach characterizes tissues through transfer learning of tissue energy interaction statistical physics models of ballistic and near-ballistic photons. The clinical information yield with our approach is comparable to conventional invasive histology. On cross evaluation with a mice model experiment, the epidermis, papillary dermis, dermis, and adipose tissue constituting the mice skin are identified with an accuracy of 99%, 95%, 99%, and 98%, respectively. This high accuracy of characterizing heterogeneous tissues using OCT justifies the ability of our computational approach to perform *in situ* histology and can be extended to regular clinical practice for diagnosis of vascular, retinal, or oral pathologies.
[DOI: 10.1117/1.JBO.18.9.090503]

Keywords: optical coherence tomography; tissue characterization; statistics of ballistic photon imaging; machine learning; *in situ* histology.

Paper 130488LR received Jul. 12, 2013; revised manuscript received Aug. 22, 2013; accepted for publication Aug. 26, 2013; published online Sep. 25, 2013.

Soft tissues like skin, fat, muscles, or blood vessels experience disorders like tumor formation, malignant growth, excess deposition of tissue components in calcification, or necrosis.[1] These affect normal functioning of the body and are medically termed as lesions. In clinical diagnosis, a small quantity of tissue from the lesion is excised using biopsy, aspiration, or exfoliation followed by the biochemical processing of the excised tissue. Subsequently, an expert histopathologist reports the tissue level abnormality by investigating the processed tissue sample under an optical microscope.[2] Although this practice is considered the gold standard, it is invasive and involves patient discomfort. Further, this practice is not feasible in critical organs like healing wounds, coronary vessels, and the eyes where biopsy is not possible in living subjects.

In clinical practice related to noninvasive evaluation of dermatological disorders and cutaneous wounds, a high degree of subjectivity exists in reporting of optical coherence tomography (OCT) used as optical biopsy.[3] Although prior studies report a high degree of concurrence between OCT images and histology,[4–6] they also report human observer-related ambiguity. Tissue characterization techniques that identify the nature of tissues based on received optical signals have been developed to reduce such ambiguity and provide histology like information.[7] Though this approach estimates the attenuation coefficients very accurately, it is not able to indicate colocated heterogeneity of tissues and the information yield is not close to conventional histology. In this work, we discuss our approach to develop an *in situ* histology technique through analysis of OCT signals and demonstrate its performance with healthy and wounded skin in swiss albino mice.

In this study, eight swiss albino mice (*Mus musculus*) (three males and five females, age 8 to 12 weeks, weight 35 to 55 g) were used. The animals were kept under a pathogen free environment in separate cages and the study was performed under the Guidelines of the Institutional Animal Care and Use Committee. Two sites per mice were selected on the dorsum, between the 6th and 8th thoracic vertebrae, symmetrically spaced 5 to 10 mm from the vertebral column [Fig. 1(a)]. The hair at these locations was removed prior to OCT imaging and a refractive index matching gel was applied to the spot for reducing signal loss at the air-epithelium junction and for increasing penetration depth.

In situ OCT imaging of mice skin [Fig. 1(c)] was performed using a swept-source OCT system (Model: OCS1300SS, Thorlabs-Inc., Newton, NJ, USA). It has a scanning-pulsed laser with the center wavelength of 1325 nm, half-power spectral bandwidth of <100 nm, axial scan rate of 16 kHz, coherence length of 6.0 mm, and average output power of 10 mW. At an imaging width of 3.0 mm and maximum imaging depth of 3.0 mm (refractive index = 1), the maximum transverse resolution was 25 μm and maximum axial resolution was 12/9 μm (air/water). The interference signal was detected using a high-transimpedence gain balanced photodetector with the noise correction. The signals were sampled and digitized using a 16-bit analog to digital converter and logarithmically compressed to 8-bit for recording. The light was focussed onto the sample surface with a long range objective while maintaining a clearance (>25 mm) between the optics and the sample. An aiming beam (660 nm) was coupled with the sample arm to locate the scanning trace of the laser [Fig. 1(a)]. Two-dimensional transverse OCT scans of the skin [Fig. 1(c)] were acquired at image resolution of 512×512 pixels corresponding to 3×3 mm^2 physical size of the imaged section.

Address all correspondence to: Debdoot Sheet, Indian Institute of Technology Kharagpur, School of Medical Science and Technology, Laboratory of Multimodal Imaging and Computing for Theranostics, Kharagpur 721302, India. Tel: +91-94740-00086; Fax: +91-3222-282-221; E-mail: debdoot@smst.iitkgp.ernet.in

0091-3286/2013/$25.00 © 2013 SPIE

Post-OCT acquisition, surgical biopsies of skin from the imaged location were collected. The biopsied tissue of approximately surface size of 5×2 mm^2 and approximately thickness of 0.5 mm (thickness of mice skin) was fixed in 4% formaldehyde solution in phosphate-buffered saline. The tissue was paraffin embedded and 4-μm thick microtomed sections were mounted on albumin coated glass slides. Each transverse section had a size of approximately 5×0.5 mm^2. Sections were deparaffinized, stained with Harris' hematoxylin and eosin (H&E),[2] and observed under a compound microscope for histological evaluation. An expert reported the histology [Fig. 1(b)] and based on these observations, the epithelium, papillary dermis, dermis, and adipose tissue were labeled on OCT scans [Fig. 1(d)] through visual correlation between them.

Post-surgical biopsy, the regenerating tissue was periodically investigated for studying the feasibility of this method in characterizing abnormal tissues. During this phase, OCT was performed on the first mice after 2 days from the day of to obtain biopsies of healthy skin. Biopsy was performed at the two sites after OCT acquisition to be used for obtaining ground truth of tissue during wound healing. Similarly, the second mouse was investigated after 4 days from the day of the first surgical biopsy. The process was followed at an interval of 2 days, such that the eighth mice was investigated after 16 days from the day of the first surgical biopsy.

We assumed $p(\omega|\mathcal{I}, \mathbf{x})$ to be the probability of finding a tissue of type ω at a location $\mathbf{x}$ in the OCT scan $\mathcal{I}$. The types of tissues considered were epithelium, papillary dermis, dermis, and adipose tissue. The probability was modeled as a response of a statistical learning function $H(\omega|\Theta, \mathcal{I}, \mathbf{x}; \{\mathcal{I}\}_{\text{train}})$ and solved using a transfer learning[8] approach. Θ at $\mathbf{x}$ defined the locally learned statistical physics knowledge of tissue-photon interaction in $\mathcal{I}$ as a multiscale model of intensity statistics and it is referred to as a source task. In target task, this knowledge was used to assign a probability value to each type of tissue ω at each location $\mathbf{x}$. We used a random forest[9] ensemble learner for this purpose along with a set of annotated samples $\{\mathcal{I}\}_{\text{train}}$.

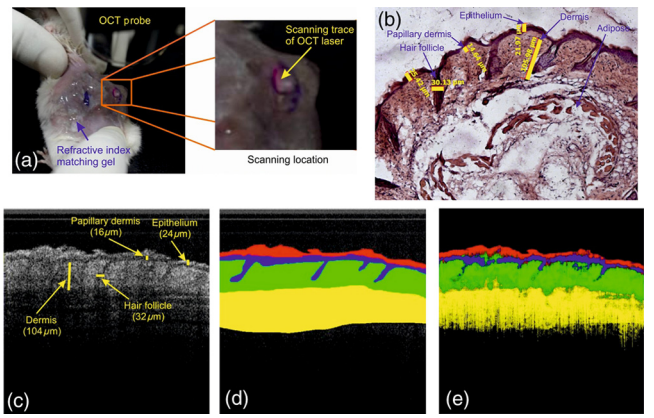

Fig. 1 Results of our proposed tissue characterization approach for *in situ* histology. (a) Photograph of the *in situ* imaging setup. The hair at the imaging has been removed and a refractive index matching gel is applied. (b) Hematoxylin and eosin (H&E) stained histology of the skin acquired using a brightfield compound optical microscope at objective magnification of 5× having pixel granularity of 1.25 μm. (c) Optical coherence tomography (OCT) image of the corresponding region. (d) The epithelium is marked in red, papillary dermis in blue, dermis in green, and adipose tissue in yellow in the ground truth image and (e) *In situ* histology visualization.

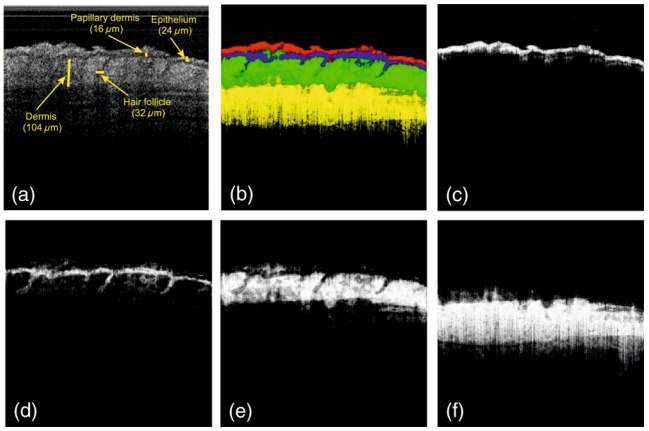

Fig. 2 Posterior probability estimated for different types of tissues: (a) OCT image of the region and (b) *in situ* histology visualization. Posterior probability for (c) epithelium, (d) papillary dermis, (e) dermis, and (f) adipose tissue.

The intensity $I_S(\mathbf{x})$ of speckle at location $\mathbf{x}$ on $\mathcal{I}$ is negatively exponentially distributed following

$$p(I_S) = 1/\sigma_S \exp(-I_S/\sigma_S),$$

with variance of σ_S.[10] Since, I_S had a high dynamic range, it was logarithmically compressed. Log-compressed signal $i(\mathbf{x})$ corresponding to $I_S(\mathbf{x})$ follows a Fisher–Tippett or double exponential distribution[11] such that $p(i; \alpha, \beta) = (1/\beta) \exp[-g - \exp(-g)]$, where $g = (i - \alpha)/\beta$. Mean (μ) and variance (σ^2) of i are related to as $\alpha = \mu + (\sqrt{6}\gamma\sigma/\pi)$ and $\beta = \sqrt{6}\sigma/\pi$, where γ is the Euler constant. The backscattering statistical physics was learned as $\{\Theta_{\text{bs}}\}$, and an ordered vector of μ and σ was estimated at multiple scales for multiscale modeling of intensity statistics, such that $\Theta_{\text{bs}} = \{(\mu, \sigma)_k\}$, where k is the scale of estimation, viz., at scale k, $(k \times k)$ number of samples centered at $\mathbf{x}$ were considered for estimating μ and σ.

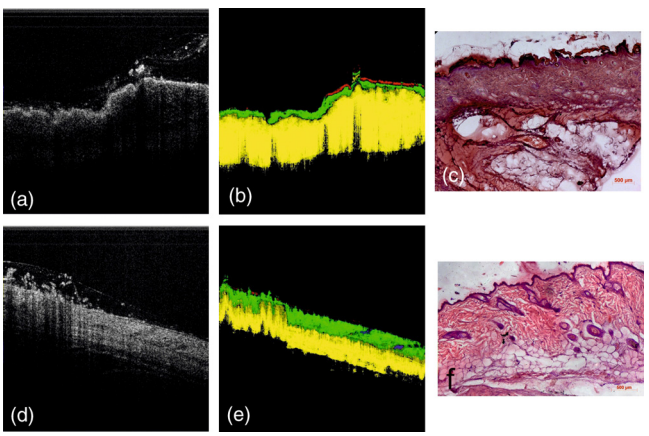

Fig. 3 Results of our proposed tissue characterization approach for *in situ* histology of abnormal tissue. (a) OCT scan of a healing surgical wound after 2 days from initial biopsy from the same site as in Fig. 1. (b) *In situ* histology of the region that depicts a thin dermis and epithelium, the papillary dermis is not yet well formed and these is an excess deposition of adipose tissue. (c) H&E stained histology of the corresponding region that correlates to the *in situ* histology image. (d) OCT scan of a healing surgical wound after 16 days from biopsy. (e) *In situ* histology of the region that depicts a well formed *dermis* and *adipose tissue*, the *papillary dermis* and *epithelium* are not yet maturely well formed. (f) H&E stained histology of the corresponding region that correlates to the *in situ* histology image.

Table 1 Percentage of correct classification and misclassification for each tissue.

		Labeled tissue			
		Epithelium	Papillary dermis	Dermis	Adipose
Ground truth	Epithelium	98.51 ± 2.43	1.33 ± 1.03	0 ± 0	0 ± 0
	Papillary dermis	0.69 ± 1.45	94.56 ± 3.53	0.21 ± 0.98	0 ± 0
	Dermis	0 ± 0	0.73 ± 1.15	99.01 ± 2.43	2.12 ± 2.77
	Adipose	0 ± 0	0 ± 0	2.54 ± 3.17	97.89 ± 2.66

The optical signals in OCT being systematically attenuated follows an exponential decay function while traversing through the tissues and the attenuation factors are tissue specific.[7] We estimated attenuation (μ_t) at each location $\mathbf{x}$ by solving the model $I_S(\mathbf{x}) = I_S(\mathbf{x}_0)\exp(-\mu_t\|\mathbf{x}-\mathbf{x}_0\|)$. Here, $\mathbf{x}_0$ and $\mathbf{x}$ were located on the same A-scan and $I_S(\mathbf{x}_0)$ was the intensity of the light incident in the skin surface at $\mathbf{x}_0$.

The tissue energy interaction modeled as Θ at $\mathbf{x}$ in the source task was the ordered set of vectors $\Theta = \{\Theta_{bs}, \mu_t\}$. Finally, given an OCT image $\mathcal{I}$ [Fig. 1(c)], using the signal value of $i(\mathbf{x})$ and Θ, the probability $p(\omega|\mathcal{I},\mathbf{x})$ of finding tissue of type ω was color coded for *in situ* histology visualization [Fig. 1(e)]. The algorithms were implemented using MATLAB (Mathworks, Natik, MA, USA) on a workstation with 12-core CPU and 384-core GPU. Source tasks were implemented on GPU and target tasks on CPU. Learning spanned about 12 s with 31 OCT scans and 0.5 s for characterizing each new scan.

In Fig. 1(e), the epithelium was very accurately predicted, while the papillary dermis was sometimes occluded by the dermis. This was possibly due to its limited spatial span. A critical comparison with the conventional histology also indicates that the predictions were more accurate than a human expert's annotations in Fig. 1(d), especially at the junction of dermis and adipose tissue. Figure 2 presents posterior probability of detecting the four different types of tissues using our proposed approach for the sample analyzed and presented in Fig. 1. The performance of this method has also been analyzed in abnormal tissue where OCT was performed on healing surgical wounds on mice skin. Figure 3(b) presents the result for a healing wound after 2 days from the time the surgical cut was made and Fig. 3(e) presents the result for a healing wound after 16 days following the surgical cut. The regeneration of tissues during healing and its progression can be evidently correlated with the corresponding histology.

We have performed a cross-validation study with a total of 32 *in situ* OCT scans and compared them with the corresponding histology. A 32-fold leave one out cross-validation was performed with the learning using 31 samples and testing on the remaining one sample. The area under receiver operating characteristics (ROC) curve was computed and found to be 0.9879 for epithelium, 0.9322 for papillary dermis, 0.9911 for dermis, and 0.9714 for adipose tissue, respectively. Additionally, an expert histologist also reported the accuracy of tissues classified using OCT signals by contrasting it with the corresponding H&E stained histology samples following a method similar to an earlier reported evaluation approach.[12] These findings are summarized in Table 1. About 98.51% of the amount of tissue labeled as epithelium by our method in the 32 OCT scan is truly epithelium as indicated in histology. There exists a standard error of 2.43% in this reporting. About 0.69% of the amount of tissue labeled as epithelium is misclassified while truly it is papillary dermis and a standard error of 1.45% exists in this reporting. About 0% of true dermis was incorrectly labeled as epithelium and 0% of true adipose was incorrectly labeled as epithelium. The rest of the table presents similar information for the other three tissue types.

We had undertaken this experiment with an initial hypothesis that photons interact characteristically with tissues and a statistical learner learning this interaction locally can provide us with an approximate information about the tissue present there. With our approach of transfer learning of tissue energy interaction in OCT of mice skin, we have been able to characterize epithelium, papillary dermis, dermis, and adipose tissue with an accuracy of 99%, 95%, 99%, and 98%, respectively, both in healthy skin and in healing wounds at different stages. We would like to extend our proposed approach for *in situ* histology of coronary vessels and oral cavity in future.

References

1. M. Miettinen, *Modern Soft Tissue Pathology*, Cambridge University Press, New York, NY (2010).
2. J. Bancroft and M. Gamble, *Theory and Practice of Histological Techniques*, Churchill Livingstone Elsevier, Philadelphia, PA (2008).
3. G. J. Tearney et al., "In vivo endoscopic optical biopsy with optical coherence tomography," *Science* **276**(5321), 2037–2039 (1997).
4. A. Barui et al., "Swept-source optical coherence tomography of lower limb wound healing with histopathological correlation," *J. Biomed. Opt.* **16**(2), 026010 (2011).
5. M. J. Cobb et al., "Noninvasive assessment of cutaneous wound healing using ultrahigh-resolution optical coherence tomography," *J. Biomed. Opt.* **11**(6), 064002 (2006).
6. T. Gambichler et al., "Comparison of histometric data obtained by optical coherence tomography and routine histology," *J. Biomed. Opt.* **10**(4), 044008 (2005).
7. G. van Soest et al., "Atherosclerotic tissue characterization in vivo by optical coherence tomography attenuation imaging," *J. Biomed. Opt.* **15**(1), 011105 (2010).
8. S. J. Pan and Q. Yang, "A survey on transfer learning," *IEEE Trans. Knowl. Data Eng.* **22**(10), 1345–1359 (2010).
9. L. Breiman, "Random forests," *Mach. Learn.* **45**(1), 5–32 (2001).
10. M. Bashkansky and J. Reintjes, "Statistics and reduction of speckle in optical coherence tomography," *Opt. Lett.* **25**(8), 545–547 (2000).
11. D. Kaplan and Q. Ma, "On the statistical characteristics of log-compressed rayleigh signals: theoretical formulation and experimental results," in *Proc. IEEE Ultrasonics Symp.*, pp. 961–964, IEEE (1993).
12. A. Katouzian et al., "Iterative self-organizing atherosclerotic tissue labeling in intravascular ultrasound images and comparison with virtual histology," *IEEE Trans. Biomed. Eng.* **59**(11), 3039–3049 (2012).